Structure
Article

Cse1p-Binding Dynamics Reveal a Binding Pattern for FG-Repeat Nucleoporins on Transport Receptors

Timothy A. Isgro[1] and Klaus Schulten[1,*]
[1] Department of Physics, University of Illinois at Urbana-Champaign, Beckman Institute for Advanced Science and Technology, Urbana, IL 61801, USA
*Correspondence: kschulte@ks.uiuc.edu
DOI 10.1016/j.str.2007.06.011

SUMMARY

Nuclear pore proteins with phenylalanine-glycine repeats are vital to the functional transport of molecules across the nuclear pore complex. The current study investigates the binding of these FG-nucleoporins to the Cse1p:Kap60p:RanGTP nuclear export complex. Fourteen binding spots for FG-nucleoporin peptides are revealed on the surface of Cse1p, and 5 are revealed on the Kap60p surface. Taken together, and along with binding data for two other transport receptors, the data suggest that the ability to bind FG-nucleoporins by itself is not enough to ensure viable nuclear transport. Rather, it is proposed that the density of binding spots on the transport receptor surface is key in determining transport viability. The number of binding spots on the transport receptor surface should be large enough to ensure multiple, simultaneous FG-repeat binding, and their arrangement should be close enough to ensure multiple binding from the same FG-nucleoporin.

INTRODUCTION

The exchange of material between the cell nucleus and cytoplasm takes place exclusively through nuclear pore complexes (NPCs), large protein assemblies embedded in the nuclear envelope (see Stewart, 2007; Lim et al., 2006a; Tran and Wente, 2006; Weis, 2003; Fried and Kutay, 2003; Macara, 2001; Rout et al., 2000 for a review). While the NPC allows for the free, unprotected exchange of small molecules (below ~40 kDa) via simple diffusion (Görlich and Kutay, 1999), it also provides a second means for the protected exchange of larger molecules between ~9 and 39 nm in diameter (Pante and Kann, 2002). This "active transport" is able to distinguish between macromolecules destined to cross the nuclear envelope and those which are not.

The overall structure of the NPC has been revealed mainly through electron microscopy (Beck et al., 2004; Stoffler et al., 2003; Kiseleva et al., 1998; Goldberg et al., 1997; Akey and Radermacher, 1993; Jarnik and Aebi, 1991; Aebi et al., 1990). The NPC has octagonal radial symmetry and pseudo two-fold symmetry across the nuclear envelope, which explains why it has such a large mass (~44 MDa in yeast [Rout et al., 2000], ~60 MDa in vertebrates [Cronshaw et al., 2002]) while containing a relatively small number (~30) of distinct proteins (Rout et al., 2000; Cronshaw et al., 2002). Larger mass estimates (Rout and Blobel, 1993; Yang et al., 1998) are likely upper limits due to the presence of NPC-associated proteins in the pore (Rout et al., 2000; Cronshaw et al., 2002).

The proteins that compose the NPC are termed nucleoporins (nups) and can be broadly separated into three categories: scaffolding, structural, and transport. Scaffolding nups contain transmembrane helices and anchor the NPC into the membranous nuclear envelope (Mansfeld et al., 2006; Schwartz, 2005). Structural nups provide the NPC its shape. They include a large subset of nups with two distinct fold types, α-solenoid and β-propellar (Devos et al., 2004, 2006). Transport nups are involved directly in the movement of complexes across the NPC. These nups are largely made up of proteins with a repeating sequence involving the amino acids phenylalanine and glycine. These FG-nups typically contain the repeating sequences FG, GLFG, or FxFG (where x is any amino acid, largely S) separated by a linker sequence of 10–20 charged or hydrophilic amino acids. Other less regularly occurring core sequences, such as SAFGxPSFG, SLFG, and SPFG, also exist (see Denning and Rexach, 2007 for a thorough analysis).

The active transport of macromolecules across the NPC involves several proteins apart from those that make up the NPC itself. A cargo macromolecule destined for transport cannot cross the NPC alone, but must associate with a chaperone transport receptor protein. These transport receptors are collectively members of the karyopherin-β family and are also known simply as karyopherins (see Pemberton and Paschal, 2005 and Mosammaparast and Pemberton, 2004 for a review). The transport complex then crosses the NPC and, once on the opposite side of the pore, dissociates, leaving the cargo in the proper compartment. The propensity of transport receptors for cargo binding or unbinding is determined by the state of Ran (GTP- or GDP-bound) on the nuclear and cytoplasmic sides of the NPC. RanGDP is present in high

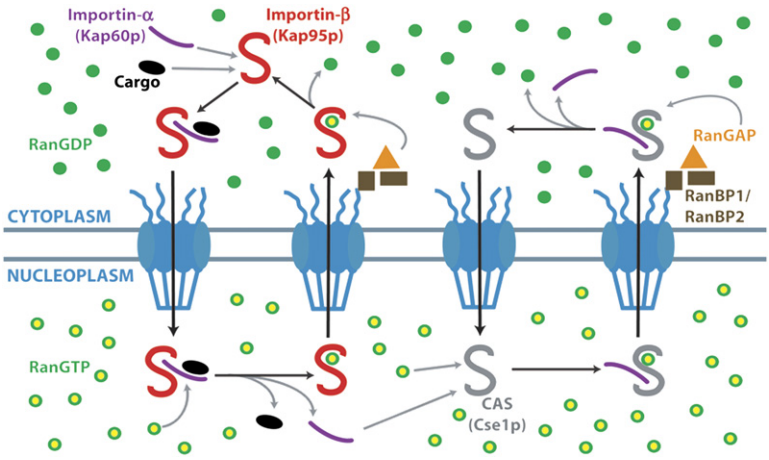

Figure 1. A Representation of Nuclear Import and Export

In order to be imported into the nucleus, a cargo macromolecule (black) must first associate in a transport complex with importin-β (red) (or another transport receptor). Protein names in yeast are shown in parentheses. This complex can then cross the nuclear pore complex into the nucleus, where the binding of RanGTP (green and yellow) causes dissociation, resulting in cargo import. Importin-β and RanGTP are then recycled to the cytoplasm, where the hydrolysis of GTP causes complex dissociation, leaving importin-β free for another round of import. The presence of the enzyme RanGTPase-activating protein, RanGAP (orange), and its accessory factors Ran-binding proteins RanBP1 and RanBP2 (brown) in the cytoplasm, causes the hydrolysis of GTP at rates much higher than the intrinsic rate. Nuclear export occurs in an analogous manner. The export of importin-α is shown. Importin-α (purple) must first associate in a transport complex with both its export receptor CAS (gray; Cse1p in yeast) and RanGTP. This complex can then navigate the nuclear pore complex and reach the cytoplasm, where the hydrolysis of GTP causes the complex to dissociate, resulting in the net export of importin-α. CAS is recycled alone to the nucleus. (The balance of Ran is reestablished by the Ran importer, NTF2, which is not shown.)

concentrations in the cytoplasm due to the presence of RanGTPase-activating protein (RanGAP), which, along with accessory factor Ran-binding proteins (RanBP1 and RanBP2), causes the hydrolysis of RanGTP at rates much higher than intrinsic (Bischoff et al., 1994, 1995a, 1995b). RanGTP is present in high concentrations in the nucleus due to the presence of the Ran guanine nucleotide exchange factor (RanGEF) RCC1, which promotes the exchange of GDP for GTP. Import receptors bind their cargo in the cytoplasm and, upon entering the nucleoplasm, release it when they bind RanGTP. Export receptors, on the other hand, only bind cargo along with RanGTP, and the complex dissociates in the cytoplasm upon hydrolysis. The restriction of RanGAP to the cytoplasm (Saitoh et al., 1998; Mahajan et al., 1997; Matunis et al., 1996; Hopper et al., 1990) and RanGEF to the nuclear chromatin (Nemergut et al., 2001; Ohtsubo et al., 1987, 1989) maintains the concentration gradients of Ran across the nuclear envelope, which is required for nucleocytoplasmic transport (Izaurralde et al., 1997; Richards et al., 1997) and imposes directionality on transport (Nachury and Weis, 1999) (see Moore, 1998 and Fried and Kutay, 2003 for a review). Furthermore, evidence exists for the role of nups in formation of intermediate states in the disassembly of transport complexes (Matsuura and Stewart, 2005; Gilchrist and Rexach, 2003). A schematic of nuclear import and export is shown in Figure 1.

Whereas much experimental data exist for the overall nuclear import and export cycle, the details of transit through the NPC are a relative mystery. However, several key pieces of information that implicate FG-nups as being vital to transport are known. Electron microscopy studies with gold-labeled antibodies have revealed that most FG-nups are localized toward the center of the NPC (Rout et al., 2000; Grote et al., 1995). Furthermore, it has also been shown that FG-nups exhibit properties similar to those of natively unfolded proteins (Denning et al., 2003), their flexibility being demonstrated directly with atomic force microscopy (Lim et al., 2006b). Moreover, FG-nups have been shown to interact with several transport receptors in vivo, in vitro, and in silico (Isgro and Schulten, 2005, 2007; Lim et al., 2007; Liu and Stewart, 2005; Cushman et al., 2004; Rodriguez et al., 2004; Morrison et al., 2003; Bednenko et al., 2003; Bayliss et al., 1999, 2000, 2002a, 2002b; Braun et al., 2002; Strawn et al., 2001; Quimby et al., 2001; Lane et al., 2000; Chaillan-Huntington et al., 2000; Damelin and Silver, 2000; Kose et al., 1999; Seedorf et al., 1999; Kehlenbach et al., 1999; Shah et al., 1998; Chi and Adam, 1997; Hu et al., 1997; Fornerod et al., 1997; Clarkson et al., 1996; Iovine et al., 1995; Paschal and Gerace, 1995; Radu et al., 1995a, 1995b; Rexach and Blobel, 1995). Another extensive study (Strawn et al., 2004) revealed that the deletion of different combinations of FG-nups rendered yeast cells inviable. While up to half of the FG-repeat mass could be deleted while still retaining a functioning NPC, the deletion of specific FG-repeat combinations was lethal. Deletion of the FG-repeat region from Nup116p alone was lethal. See Tran and Wente (2006) for a review of FG-nups and the manner in which they facilitate transport. Several theories have been proposed to explain the mechanism of nucleocytoplasmic transport through the NPC (Peters, 2005; Rout et al., 2000, 2003; Shulga and Goldfarb, 2003; Ribbeck and Görlich, 2001; Ben-Efriam and Gerace, 2001; Macara, 2001).

While a large body of evidence detailing the interactions of several transport receptors with FG-nups has been uncovered, not much study has been devoted to the yeast transport receptor Cse1p (CAS in vertebrates), whose crystal structure is available in complex with Kap60p (importin-α) and RanGTP (Matsuura and Stewart, 2004) and in cargo-free form (Cook et al., 2005). Cse1p functions as the Kap60p exporter (Solsbacher et al., 1998; Hood

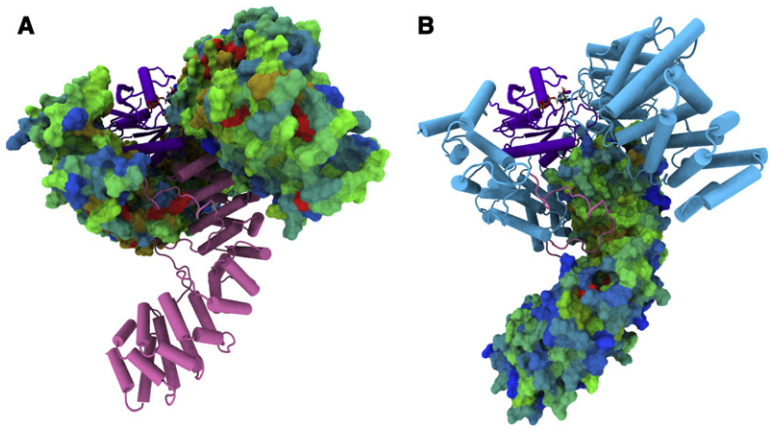

Figure 2. Two Views of the Cse1p:-Kap60p:RanGTP Nuclear Export Complex

(A) Cse1p is shown with its solvent-accessible surface colored according to conserved hydrophobic amino acids, as described in Experimental Procedures. Cse1p makes intimate contact with Kap60p (pink) and Ran (purple) in complex with GTP. The ten ARM repeats that compose Kap60p are apparent.

(B) The same view of the complex; Cse1p is shown in cartoon, and the Kap60p surface is now colored by conserved hydrophobic amino acids. Kap60p shows less overall conservation of surface hydrophobic amino acids.

and Silver, 1998; Künzler and Hurt, 1998; Kutay et al., 1997), recycling the protein back to the cytoplasm after it assists in nuclear import as an adaptor for Kap95p (importin-β). The recycling of Kap60p is initiated by the binding of Nup2p (Nup50) to Kap60p, displacing a bound nuclear localization signal (NLS) (Matsuura and Stewart, 2005; Matsuura et al., 2003; Gilchrist et al., 2002), after which Cse1p binds to Kap60p and displaces Nup2p.

Cse1p is a right-handed superhelical protein composed of 20 HEAT repeats. Kap60p is comprised primarily of ten Armadillo (ARM) repeats, along with an N-terminal region that lacks secondary structure and includes the importin-β-binding domain of the protein. In the export complex, RanGTP and ARM repeats 8–10 of Kap60p are clamped between the N- and C-terminal arches of Cse1p, with contact between Ran and ARM repeat 10. Kap60p ARM repeats 1–7 protrude away from Cse1p. The complex is shown in Figure 2.

This study utilized molecular dynamics to study interactions between FG-nup peptides and the Cse1p:Kap60p:RanGTP export complex. Four simulations were performed with the transport complex in an aqueous environment containing FG-nup peptides that were 4–10 amino acids long; the sequences of these peptides were taken from Nsp1p and Nup116. The simulations are summarized in Table S5 (see the Supplemental Data available with this article online), and the peptides used are listed in Table 1. During the course of simulation, FG-nup peptides diffuse through solution, and some bind to the transport complex surface. Movie S1 in Supplemental Data shows the binding of FG-nup peptides over the course of simulation 1. The simulations revealed 14 binding spots for FG-repeat peptides on the surface of Cse1p and 5 binding spots on the surface of Kap60p. Taken together and with results from previous binding spot studies, the results reveal that viable transport across the NPC may be dependent on the arrangement of binding spots in clusters on the transport receptor surface.

RESULTS

The current binding simulations reveal FG-nup peptides diffusing through the aqueous environment around the Cse1p:Kap60p:RanGTP export complex, with some peptides interacting with the surface of the complex. In order to determine which surface interactions, occurring on the order of tens of nanoseconds, could be classified as relevant in vivo, on the order of microseconds or milliseconds, three criteria were employed: the binding should occur until the end of the simulation; the binding should occur in a depressed cavity on the protein surface, as opposed to a flat surface; and the binding should occur at a conserved and hydrophobic spot on the complex surface. The last criterion was formed by aligning sequences of Cse1p and Kap60p to score each residue based on conservation. It is fully described in Experimental Procedures. This criterion was not rigorously enforced if the binding of FG-nup peptides was sufficiently strong based on visual inspection and occurred for a long enough period of time.

Binding of FG-nup peptides was observed on 14 spots on the Cse1p surface. Binding is concentrated between HEAT repeats 10 and 16, with 8 of the 14 binding spots appearing in that region, and 1 or more binding spots for each crevice between repeats. Binding of FG-nup peptides to Kap60p, on the other hand, appears to be much less extensive and sparser than on the Cse1p surface. Binding was observed at five spots on the Kap60p surface, indicating a much lesser concentration in binding spots than seen on the Cse1p surface. A schematic of FG-nup peptide binding to both the Cse1p and Kap60p surface can be seen in Figure 3.

The concentration of binding spots combined with the regularity in spacing of HEAT repeats on the Cse1p surface may indicate a means by which the NPC recognizes and binds transport receptors while not doing so for inert proteins. The large amount of regularly spaced binding spots may provide the proper complementarity for binding a single, long FG-nup with regularly spaced FG-repeats (or a few FG-nups). The binding of multiple FG-repeats from one FG-nup would also serve to strengthen an otherwise weak single FG-repeat:transport receptor interaction. Evidence exists for the binding of 2 Phe residues from a single FG-nup to two spots on the surface of the transport receptor importin-β (Liu and Stewart, 2005). This FG-nup "multiple binding" may be necessary for nuclear transport.

Table 1. Summary of the FG-Nup Peptides Used in the Simulations

Nsp1 Sequence	Sequence Label	Nsp1 Residues	Nup116 Sequence	Sequence Label	Nup116 Residues
KTPFSFGTAN	#N10	10–19	TTGGLFGQKP	#U202	202–211
KPAFSFGATT	#N176	176–185	NSTGLFGSST	#U232	232–241
TTGFSFGSQL	#N214	214–223	TSGGLFGNTT	#U256	256–265
TPSFSFGAKS	#N281	281–290	NNTGLFGQQN	#U273	273–282
KPAFSFGAKP	#N300	300–309, 338–347	TNGGLFGQQQ	#U285	285–294
		376–385, 509–518	ASGGLFGQSA	#U356	356–365
KPAFSFGAKS	#N319	319–328, 357–366	TTGGLFGQTN	#U379	379–388
		414–423, 452–461	SGGGLFGQQQ	#U392	392–401
		471–480	NAGGLFGQNN	#U404	404–413
KPAFSFGAKA	#N528	528–537	NQSGLFGQQN	#U417	417–426
KSAFSFGSKP	#N547	547–556	QQGGLFGSKP	#U436	436–445
FSFG	4N	—	PAGGLFGQQQ	#U445	445–454
			STGGLFGQQN	#U479	479–488
			QPGGLFGQTN	#U494	494–503
			ASGGLFGSKP	#U569	569–578
			VGGGLFGNNQ	#U582	582–591
			TSGGLFGSKP	#U610	601–610
			NSTGLFGNKP	#U645	645–654
			SAGGLFGNNN	#U662	662–671
			GSTGLFGSNN	#U680	680–689

Each simulation used 111 individual peptides to yield an FG concentration of ~60 mM. Simulation 1 used simple FSFG peptides. Simulations 2, 3, and 4 used FG-nup peptides that were 6, 8, and 10 amino acids in length, respectively, and were taken from nucleoporins Nsp1 and Nup116. The nup sequences listed are those that appear in simulation 4. For simulation 3, one amino acid was trimmed off the ends of these sequences, and for simulation 2, two were trimmed. The following nomenclature is used in labeling sequences: number of amino acids–nup identifier (i.e., first residue in 10 aa long chain). For example, the chain PFSFGT in simulation 2 is referred to as 6N10. There are 8 Nsp1 sequences listed (comprising 15 Nsp1 chains; chain N300 is duplicated 4 times, and chain N319 is duplicated 5 times) and 20 distinct Nup116 sequences. (Redundancy in both Nsp1 and Nup116 increases as chains are shortened.) For simulations 2, 3, and 4, each chain is present in solution three times, along with an extra copy of chains N10, N176, N214, and N281. Simulation 2 also had an extra copy of chains 6N547 and 6U232, simulation 3 had an extra copy of 8N300 and 8N547, and simulation 4 had an extra copy of 10N300 and 10N319, yielding 111 peptides for each simulation.

Cse1p Binding

Binding spot #1 on the Cse1p surface exists between HEAT repeats 2/3 near the conserved and hydrophobic residue Leu93. Residues Phe6 and Leu5 from peptide 10U379 bind to the spot for ~17 ns during simulation 4. The Phe6 and Leu5 side chains rest on the Cse1p surface, and Phe6 is embedded between the side chains of Ser96 and Ala45. The residues Ser46, Thr47, and His42 protrude from the Cse1p surface, providing a surface on which much of the peptide backbone adheres. Binding spot #1 can be seen in Figure 4A.

Binding spot #2 exists between HEAT repeats 4/5 and is composed of residues centered around Ile201 and Leu202. Although not strictly conserved across all ten species, Ile201 is aligned with a similar Val in eight of the nine species, and Leu202 is conserved in all but one species (replaced with Ile). Asp135, Gln188, and Asn192 surround the Phe3 aromatic ring side chain of peptide 4N, which is buried in the pocket, adhering to the hydrophobic residues at its base. Phe3 binds to the spot for ~19 ns during simulation 1. The binding spot can be seen in Figure 4B.

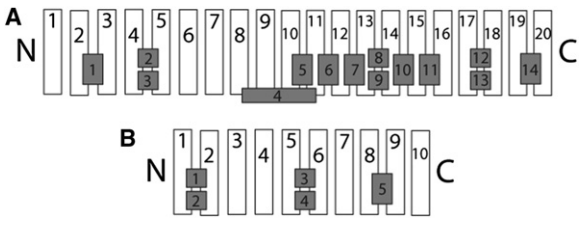

Figure 3. A Schematic Representation of FG-Nup Binding Spots on the Surfaces of Cse1p and Kap60p

(A) Cse1p HEAT repeats 1–20 are represented in the schematic and labeled. The 14 binding spots revealed by the present study are also labeled as dark boxes and numbered.

(B) Kap60p ARM repeats 1–10 are labeled, as are the five binding spots revealed by the current simulations.

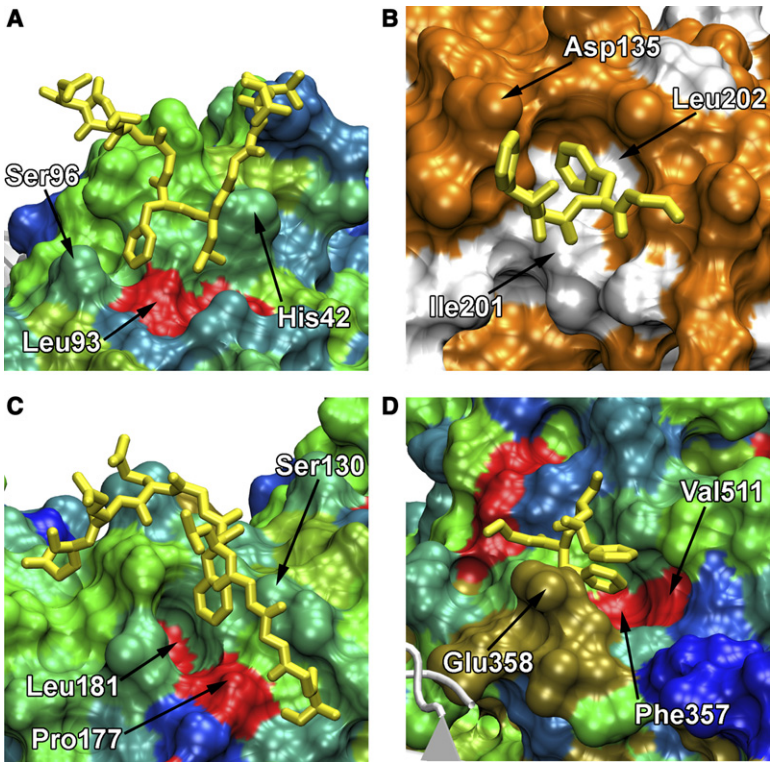

Figure 4. Binding of FG-Nup Peptides to Binding Spots #1–#4 on the Cse1p Surface

(A–D) In (A), (C), and (D), the Cse1p surface is colored by residue conservation and hydrophobicity. Red residues are completely conserved and hydrophobic, while blue residues are nonconserved. See Experimental Procedures for details. In (B), the surface is colored by hydrophobicity. White residues are hydrophobic, and all others are colored orange. (A) Binding spot #1 is located between HEAT repeats 2/3 and is formed by residues Leu93, Ser96, Ala45, Ser46, Thr47, and His42. Residues Phe6 and Leu5 from peptide 10U379 are shown bound to the spot at the end of simulation 4. (B) Binding spot #2 is formed by residues Ile201, Leu202, Asp135, Gln188, and Asn192 between HEAT repeats 4/5. Peptide 4N is shown bound to the spot at the end of simulation 1. (C) Binding spot #3 is composed of residues Pro177, Leu181, Ser130, Leu132, Ser133, and Asn134, also between HEAT repeats 4/5. Phe6 from peptide 10U392 is shown bound to the spot at the end of simulation 4. (D) Binding spot #4 is formed by residues Phe357, Val511, Ile472, and Glu358 from HEAT repeats 8, 10, and 11. Peptide 4N is shown bound at the end of simulation 1.

Binding spot #3 is also between HEAT repeats 4/5, but it is centered on the conserved and hydrophobic residues Pro177 and Leu181. Residues Ser130, Leu132, Ser133, and Asn134 surround residue Phe6 from peptide 10U392, which binds to the spot with its side chain ring for ~16 ns during simulation 4. The binding spot can be seen in Figure 4C.

Binding spot #4 is not located on the convex face of Cse1p, but rather on the "side" of the molecule, between its convex and concave faces. The binding spot is also unique in that it is located between three HEAT repeats: 10/11, and the long insert region of HEAT repeat 8. Phe357 and Val511 form the base of the binding spot, with residues Ile472 and Glu358 binding the side chain ring of Phe3 from peptide 4N. The peptide binds for ~33 ns during simulation 1, and the spot is shown in Figure 4D.

Binding spot #5 is located between HEAT repeats 10/11, is centered on the hydrophobic residue Phe504, and is near the conserved Leu464. Residue Phe4 from peptide 10N300 is observed in simulation 4 to bind for ~7 ns. The aromatic ring of Phe504 composes the base of this binding spot and provides its hydrophobicity along with Ile500. Residues Thr503 and Gln506 compose one side of the binding spot, and Asn467 and Ser466 compose the other. However, the binding spot appears viable primarily due to favorable interaction between Phe4 and Phe504 side chain rings. The binding spot is shown in Figure 5A.

Binding spot #6 is located between HEAT repeats 11/12 near the conserved and hydrophobic Pro499. Residues Phe537, Asp541, Ser545, Met498, and Ile495 compose a very deep and narrow pocket in which the side chain ring of Phe1 from peptide 4N rests. The narrow pocket ensures a very tight bind for the flat aromatic Phe ring. Binding is observed in simulation 1 for ~32 ns. The Phe1 side chain of the 4N peptide is first recruited to the spot, binds between residues Phe499 and Ser545 and Ile548 for ~27 ns, and then migrates toward Phe537 upon a conformational change of the Met498 side chain, spending the last ~5 ns of simulation 1 in the conformation shown in Figure 5B.

Binding spot #7 is located between HEAT repeats 12/13 near the conserved Pro590. The spot is composed of two separate binding "pockets" in close proximity to each other. Binding to the spot is observed in simulations 1 and 3. In simulation 1, peptide 4N binds to pocket #1 for the last ~34 ns. The pocket is composed mainly of residues classically considered to be hydrophilic: Glu547, Lys551, and Gln594. The side chains from these residues protrude from the Cse1p surface along with Leu591, forming the sides of the binding pocket. Despite the fact that the end of each side chain contains a charge, the middle, aliphatic portion of each side chain yields a pocket with a large hydrophobic character, suitable for the Phe1 side chain ring from peptide 4N. Ile554 and Leu595 form the base of the binding spot, further increasing its hydrophobicity. The formation of a hydrophobic binding spot for FG-repeats from classically hydrophilic residues has also been observed in the transport receptor NTF2 (binding spot #5) (Isgro and Schulten, 2007). In simulation 3, Phe3 from peptide 8N300 binds to pocket #2 of binding spot #7 for ~28 ns. In this case, interaction with the Phe3 side chain ring is limited to residues Pro590, Thr546,

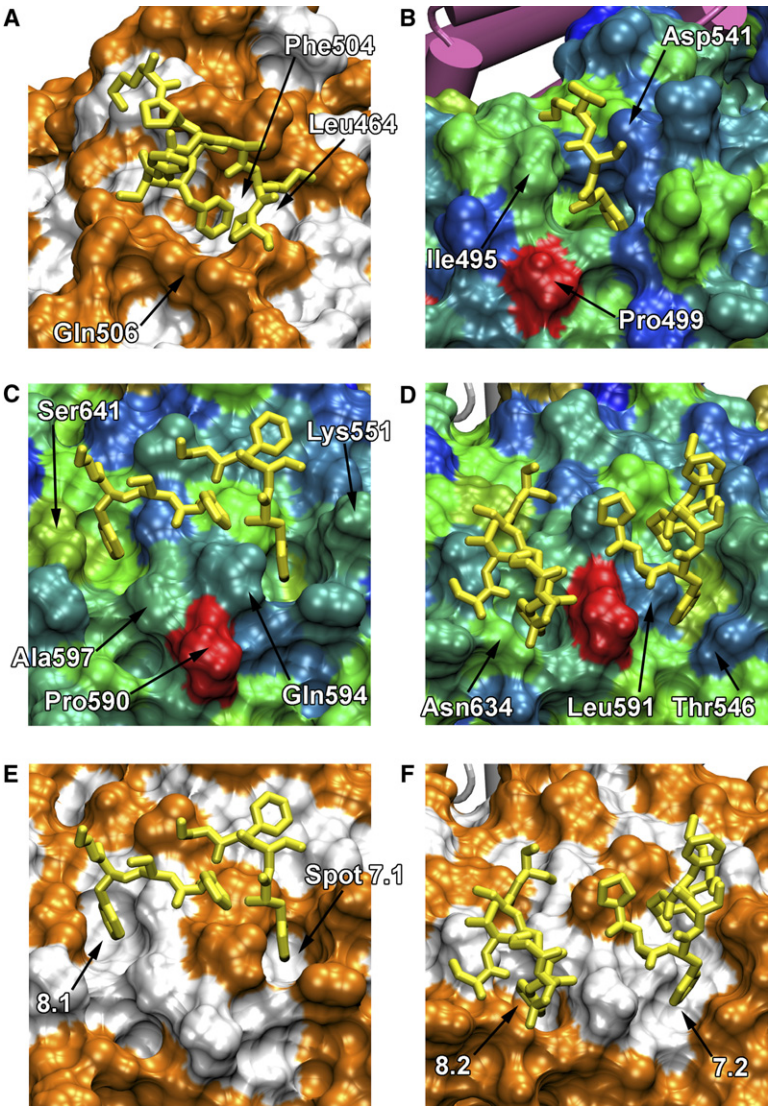

Figure 5. Binding of FG-Nup Peptides to Spots #5–#8 on the Cse1p Surface

(A) Binding spot #5 is formed by resides Phe504, Leu464, Ile500, Thr503, and Gln506 between HEAT repeats 10/11. The binding spot is shown at the end of simulation 4 with peptide 10N300 bound.

(B) Binding spot #6 is formed by residues Phe537, Asp541, Ser545, Met498, and Ile495 between HEAT repeats 11/12. It is shown with peptide 4N bound at the end of simulation 1. Kap60p is visible in pink in the background.

(C–F) Binding spots #7 and #8 are shown at the end of (C and E) simulations 1 and (D and F) 3; the Cse1p surface is colored according to (C and D) conservation and (E and F) hydrophobicity. Each binding spot contains a second pocket, labeled in (F).

Leu591, and Ile588. Both binding pockets, i.e., #1 and #2, are located on either side of Leu591. Binding to both pockets and their positions relative to one another (and to binding spot #8) are indicated in Figures 5C–5F.

Binding spot #8 is very similar to spot #7 in that it is also composed of two binding pockets near the conserved and hydrophobic residue Pro590. Binding to the pockets is also observed in simulations 1 and 3, but they are located between HEAT repeats 13/14. Binding to pocket #1 is observed in simulation 1. Phe3 from peptide 4N binds to the spot for ~25 ns. The Phe3 side chain ring is sandwiched between Cse1p residues Ala597 and Pro593 on one side and Ser641 on the other. Residues Leu638 and Ile600 form a hydrophobic bottom for the binding pocket. Peptide 8U232 binds to pocket #2 for ~21 ns during simulation 3. Residue Phe5 from the peptide binds to the pocket that is composed of residues Pro593, Pro590, and Gln589 on one side of the Phe side chain ring and Leu637 and Asn634 on the other. Residues Leu638 and Thr630 form the base of the pocket. Figures 5C–5F show both binding pockets from spot #8 in relation to one another and to binding spot #7.

Binding spot #9 is also located between HEAT repeats 13/14, though on the opposite side of the convex face of Cse1p from binding spot #8. Residue Phe4 from peptide 6U436 binds to the spot for ~16 ns during simulation 2. Residues Ala607, Ile654, and Val649 form a hydrophobic base for the binding spot, and the Phe4 ring lies parallel to the Kap60p surface on top of them. Residues Thr604, Thr648, and Glu652 surround this base and provide protection for the peptide from the aqueous environment. Figure 6A shows peptide 6U436 binding to the spot at the end of simulation 2.

Binding spot #10 is located between HEAT repeats 14/15 and is observed in simulations 1, 3, and 4. The spot is centered on the conserved and hydrophobic residue Leu682. The spot is composed primarily of Leu682 and the large residues Phe650, Phe652, and Pro685, which provide a deep and hydrophobic pocket for FG-nup binding. In simulation 1, the side chain ring of Phe1 from

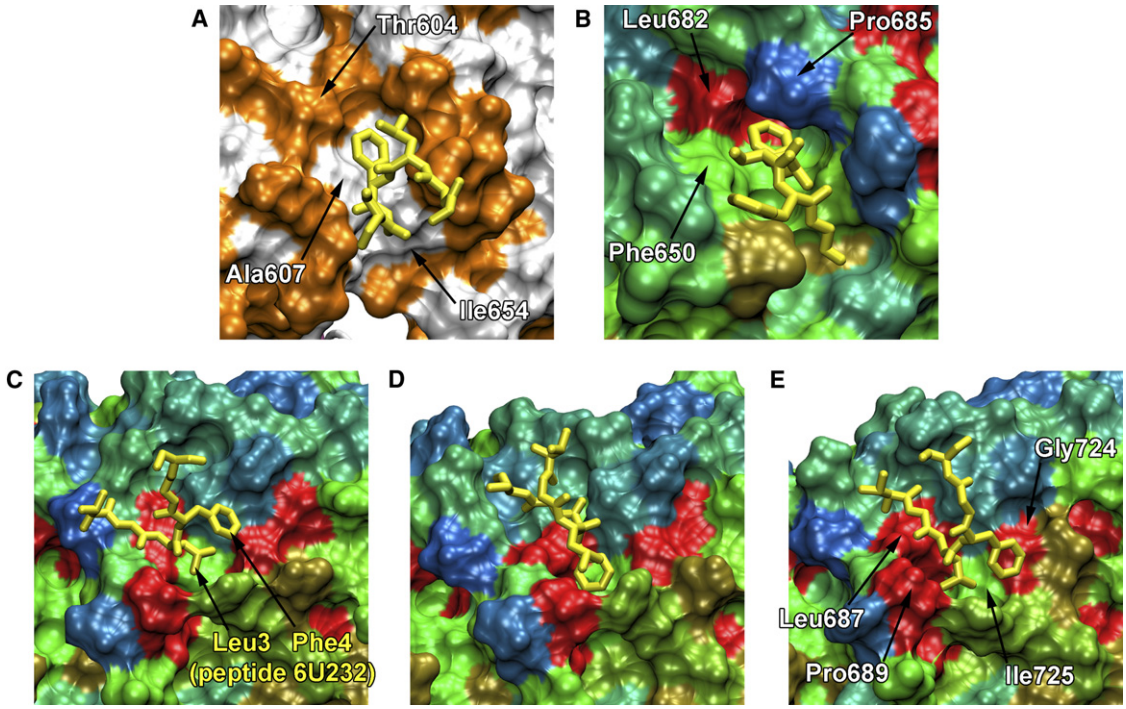

Figure 6. Binding of FG-Nup Peptides to Spots #9–#11 on the Cse1p Surface

(A) Binding spot #9 is located between HEAT repeats 13/14 and is formed by residues Ala607, Ile654, Val649, Thr604, Thr648, and Glu652. The binding spot is shown at the end of simulation 2 with Phe4 from peptide 6U436 bound.

(B) Binding spot #10 is formed by residues Leu682, Phe650, Phe652, and Pro685 between HEAT repeats 14/15. The binding spot is shown at the end of simulation 1.

(C) Binding spot #11 is shown after 9 ns have passed in simulation 2; Leu3 from peptide 6U232 occupies the binding spot. The binding spot is composed of residues Pro689, Ala688, Leu687, Pro721, Gly724, Arg728, and Ile725 between HEAT repeats 15/16.

(D) Binding spot #11 after 17 ns have passed, now with Phe4 from 6U232 occupying the binding spot.

(E) Binding spot #11 at the end of simulation 2, with both Leu3 and Phe4 occupying the binding spot.

peptide 4N is buried in the binding spot for ~22 ns, making intimate contact with both Phe650 and Phe652. Figure 6B shows the binding spot, along with the Phe-Phe peptide-Cse1p contact.

Binding spot #11 is located between HEAT repeats 15/16 and is composed of a group of conserved and hydrophobic residues, including Pro689 and Leu687. Binding of the peptide 6U232 to this spot for ~34 ns, the majority of the 37.2 ns simulation, is observed in simulation 2. Binding occurs via both residues Leu3 and Phe4 of the 6U232 peptide, with the two switching positions twice throughout the simulation. The binding spot is a broad hydrophobic pocket on the Cse1p surface composed of residues Pro689, Ala688, Leu687, Pro721, Gly724, and Arg728. Ile725 composes the bottom of the pocket. Binding is initiated in the pocket by the Leu3 side chain, which remains bound for ~9 ns, after which time it is replaced by the Phe4 ring. The Phe4 side chain then occupies the binding spot for the next ~12 ns and is subsequently replaced by Leu3 for the remaining ~13 ns. The hydrophobic volume occupied by both the Leu3 and Phe4 side chains appears too large for the binding spot to accommodate the two simultaneously. We hypothesize that a nup peptide with an FSFG core may have higher affinity for this binding spot due to the difference in the size of the Ser and Leu side chains. Figures 6C–6E show the binding spot at three different times during the course of simulation 2.

Binding spot #12 is located between HEAT repeats 17/18 and is observed in simulations 2, 3, and 4. The binding spot is composed of residues Phe797, His800, Met752, and Arg756, which roughly form the sides of the binding spot, and Ile759 as the base. While the residues that compose binding spot #12 are not conserved across Cse1p species, we propose that the binding spot is relevant in vivo due to observed binding in three of the four simulations. Figure 7A shows the binding spot at the end of simulation 3, in which binding of the Phe5 aromatic ring from peptide 8N176 occurs for ~8 ns.

Binding spot #13 is also located between HEAT repeats 17/18. This binding spot, however, is centered on the residues Phe817 and the conserved Leu770. It is a hydrophobic channel that is able to bind two FG-nup peptides at once, as observed in simulation 1. Pocket #1 is composed of the hydrophobic residues Leu770, Phe817, Leu767, and Leu809, as well as the aliphatic part of the Gln771 and Gln812 side chains. Phe1 from a 4N peptide binds to the spot for ~9 ns. On the opposite side of Phe817 (see Figure 7), residues Lys774, Val779, Thr820, and

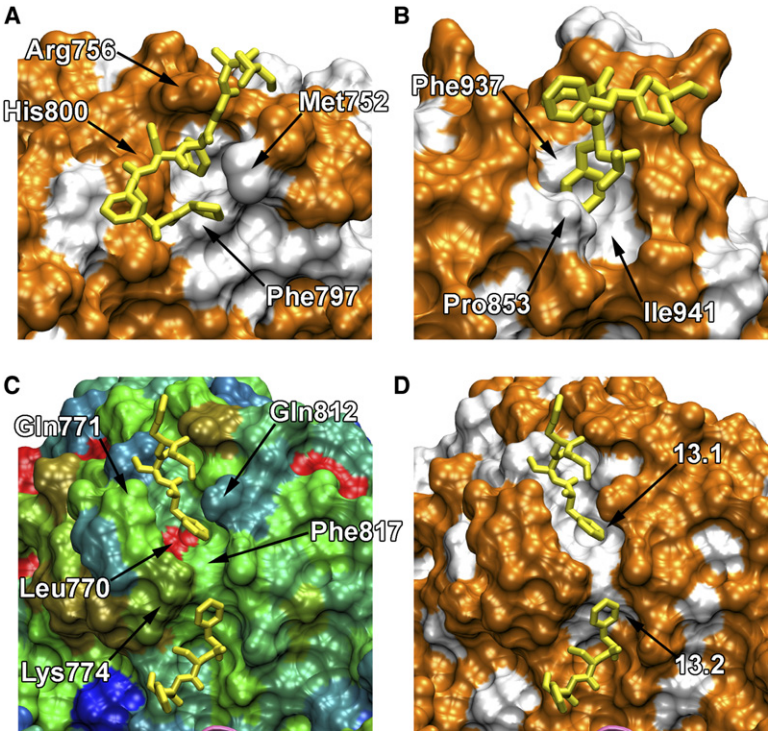

Figure 7. Binding of FG-Nup Peptides to Spots #12–#14 on the Cse1p Surface

(A) Binding spot #12 shown at the end of simulation 3 with peptide 8N176 bound. The binding spot is located between HEAT repeats 17/18 and is composed of residues Phe797, His800, Met752, Arg756, and Ile759.

(B) Binding spot #14 shown at the end of simulation 2 with peptide 6N176 bound. The binding spot is composed of residues Phe937, Ile856, Ile941, Pro853, Gln849, and Thr940 and is located between HEAT repeats 19/20.

(C) Binding spot #13 shown at the end of simulation 1 and colored according to conservation. The binding spot is composed of two binding pockets, capable of binding two FG-repeats, as shown. The binding spot is located between HEAT repeat 17/18 and is centered on residue Phe817.

(D) Binding spot #13 is colored according to hydrophobicity; the two binding pockets are labeled.

Asn816 form pocket #2, along with Phe817. Phe1 from another 4N peptide binds to the pocket for ~17 ns. Figures 7C and 7D show both pockets from binding spot #13 at the end of simulation 1 with both 4N peptides bound.

Binding spot #14 is located between HEAT repeats 19/20 and is centered on Phe937. The hydrophobic character of the spot arises due to the presence of Phe937, Ile856, and Ile941, which compose the base of the binding spot. Pro853, Gln849, and Thr940 compose the walls of the binding spot and serve to envelop the Phe2 side chain ring of peptide 6N176 for ~5 ns during simulation 2. The binding spot is shown in Figure 7B.

Kap60p Binding

Binding of the non-FG N-terminal domain of Nup50p (Nup2p in yeast) to importin-α (Kap60p) has been shown to displace NLSs and thus catalyze import complex dissociation and importin recycling (Matsuura and Stewart, 2005; Matsuura et al., 2003; Gilchrist et al., 2002). The extensive binding of nup FG-repeat regions to the surface of Kap60p is not expected, however, given that the molecule requires Cse1p for recycling and cannot navigate the NPC on its own. This is also reflected in the lack of conserved and hydrophobic regions on the Kap60p surface compared to the Cse1p surface (see Figure 2). Indeed, three out of the five spots described below are located at residues not conserved across all ten species.

The current simulations reveal five binding spots on the surface of Kap60p. The binding spots are relatively sparse over the ARM repeats 1–10 in comparison to Cse1p FG-nup binding.

Binding spot #1 is located between ARM repeats 1/2 on the concave surface of Kap60p. Residue Phe1 from peptide 4N binds to the spot, which is centered on the conserved and hydrophobic residue Leu115, for ~13 ns in simulation 1. The spot is composed of residues Ile123, Pro121, Thr162, Gly161, Ser160, and Arg56.

Binding spot #2 is also located between ARM repeats 1/2, near the end of the molecule, and is centered on residue Val125. Binding to this spot was observed in simulations 2 and 3. The spot is composed of the small and hydrophobic residues Leu89, Val125, Ala129, and Pro90, along with residues Gln128 and Asp124. In simulation 2, residue Phe4 from peptide 6N214 lays its aromatic ring in a hydrophobic channel formed by these residues, where it sits bound for ~24 ns.

Binding spot #3 is located between ARM repeats 5/6. The spot is centered on residue Ala263 and takes a portion of its hydrophobic character from the aliphatic portion of the Lys264 and Arg299 side chains. Binding to this spot is observed in simulations 2 and 4. Binding in simulation 2 occurs via the side chain ring of residue Phe2 from peptide 6N281 for ~22 ns. The aromatic ring lies between Lys264 and Arg299, and lies parallel to the Kap60p surface on top of residues Val298 and Ala263, and next to Tyr267.

Binding spot #4 is also located between ARM repeats 5/6, but on the "side" of the repeats, near the conserved and hydrophobic Leu284. Binding of peptide 4N is observed in simulation 1, whereby the Phe1 side chain ring becomes sandwiched between residues Val255 on one side and Ala291 on the other for ~4 ns. Residues Ala294 and Trp252 also likely contribute to the hydrophobic quality of this binding spot.

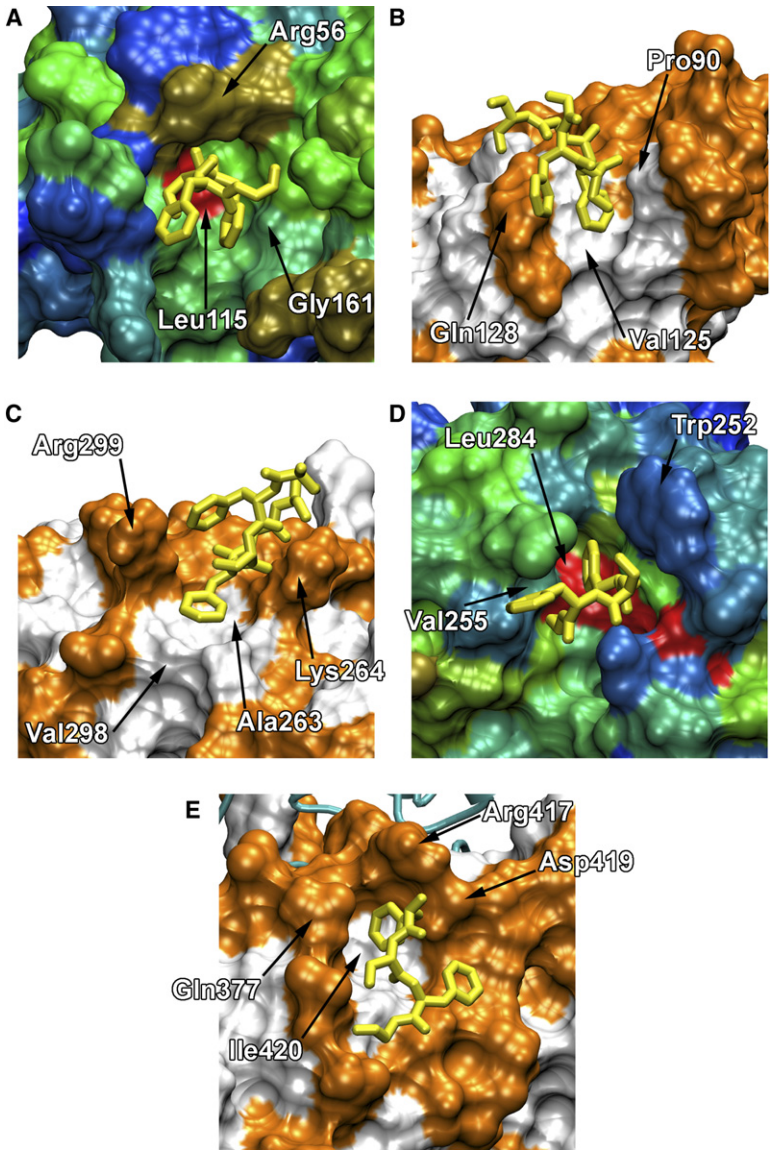

Figure 8. Binding of FG-Nup Peptides to the Kap60p Surface

(A) Binding spot #1 is located between ARM repeats 1/2 on the concave surface of Kap60p and is composed of residues Ile123, Pro121, Thr162, Gly161, Ser160, and Arg56. It is shown at the end of simulation 1.

(B) Binding spot #2 is also located between ARM repeats 1/2 and is composed of residues Leu89, Val125, Ala129, Pro90, Gln128, and Asp124. It is shown at the end of simulation 2.

(C) Binding spot #3 is located between ARM repeats 5/6 and is composed of residues Lys264, Arg299, Val298, Ala263, and Tyr267. It is shown at the end of simulation 2.

(D) Binding spot #4 is also located between ARM repeats 5/6, but on the "side" of the ARM repeats, centered on the conserved residue Leu284. It is shown at the end of simulation 1.

(E) Binding spot #5 is located between ARM repeats 8/9, and is composed of residues Ile380, Ile420, Tyr423, Arg417, Asp419, and Gln377. It is shown at the end of simulation 1.

Binding spot #5 is located between ARM repeats 8/9. Binding to this spot is observed in simulations 1 and 3. The binding spot is composed of a base of hydrophobic residues Ile380, Ile420, and the large aromatic ring of Tyr423. Residues Arg417 and Asp419 form a salt bridge to one another with their side chains, which protrude roughly perpendicular from the Kap60p surface. This leaves the large, aliphatic portion of the Arg417 and Asp419 side chains adjacent to the hydrophobic base of the binding spot, further contributing to its hydrophobicity. Residue Phe1 from peptide 4N binds to this spot for ~16 ns in simulation 1, and its side chain ring is shielded from the aqueous environment by the Arg-Asp aliphatic side chains as well as by the aliphatic portion of Gln377 on its opposite side. Figure 8 shows each of the Kap60p binding spots described.

The sparse (but not nonexistent) binding of FG-nup peptides on the Kap60p surface suggests that binding of FG-nups alone is not sufficient to allow for macromolecule transport through the NPC. Rather, the large number of FG-nup binding spots on the Cse1p surface, notably in the HEAT 10–16 region, in comparison to the Kap60p surface, implies that the number of binding spots on the transport receptor surface and the distance between them may be crucial factors in determining NPC binding and transport.

DISCUSSION

The present simulations reveal 14 binding spots for FG-nup peptides on the Cse1p surface and 5 binding spots on the Kap60p surface. The simulations provide a unique insight into how the nuclear pore likely recognizes a transport receptor (and cargo) destined for nuclear import while preventing the transport of inert macromolecules. Comparing the binding spots on the Kap60p surface and the

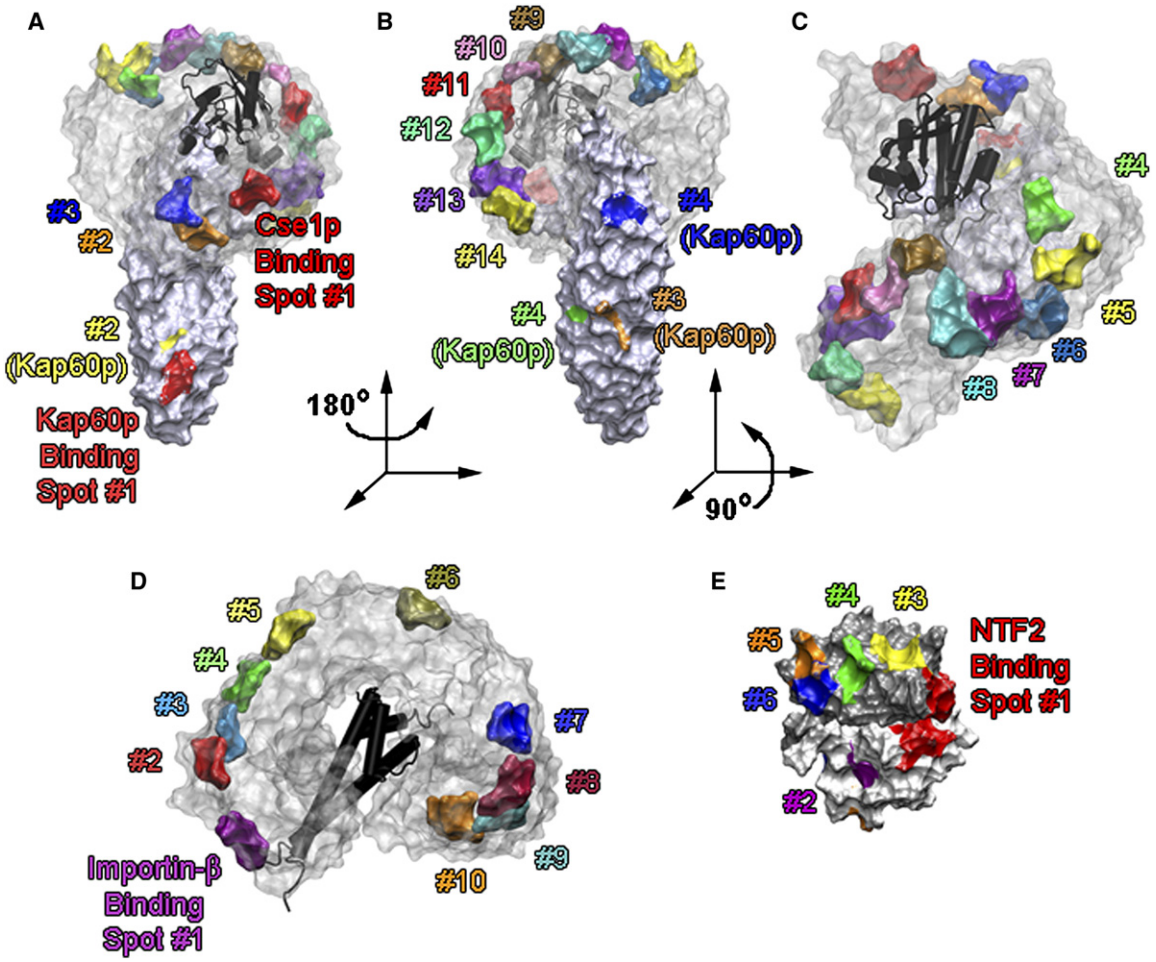

Figure 9. Location of FG-Repeat Binding Spots on the Surface of Cse1p, Importin-β, NTF2, and Kap60p

(A) A view of the Cse1p:Kap60p:RanGTP export complex with the solvent-accessible surface of Cse1p shown transparently for clarity in showing the proximity of binding spots (colored and labeled). The Kap60p surface is colored blueish-white; binding spots are shown in color and are labeled as well. RanGTP is shown in black. Movie S2 shows a rotating 3D view of these data.

(B) Rotated 180° about the vertical axis.

(C) Rotated 90° about the horizontal axis. The large binding spot cluster at the start of the C-terminal half of the molecule is apparent (spots #4–#11).

(D) A view of importin-β in complex with part of its cargo SREBP-2 (Lee et al., 2003). The importin-β surface is shown transparently for clarity in showing binding spots, which are numbered as in Isgro and Schulten (2005). Note the N-terminal and C-terminal binding spot clusters, spots #2–#5 and #7–#10, respectively. SREBP-2 helices are shown in black. Movie S3 shows a rotating 3D view of these data.

(E) A view of the NTF2 dimer surface (Bayliss et al., 2002a); one monomer is shown in gray, one is shown in white, and binding spots are shown in color. Binding spots #1 and #3–#6 form a broad stripe across the NTF2 surface. Binding spots are numbered as in Isgro and Schulten (2007). The three transport receptors are not to scale with respect to one another, but Cse1p is with respect to itself. Movie S4 shows a rotating 3D view of these data.

Cse1p surface reveals a striking difference, not simply in the number of binding spots, but most notably in their orientation on the surface of each protein.

The relatively small amount of Kap60p binding spots yields a lower average binding spot density across the entire protein surface than across that of Cse1p. Furthermore, the Kap60p binding spots are also spread widely across the protein's surface, from ARM repeat 1 to 9 (see Figure 9 and Movie S2), with no more than two binding spots clustered at short distances (see Table S2). The location of Cse1p binding spots, on the other hand, appears in three broader clusters across the surface, the most populated one near the beginning of the C-terminal half of the molecule: 8 of the 14 Cse1p binding spots are located in this cluster between HEAT repeats 10 and 16 (spots #4–#11). The binding spots in this cluster are separated from their neighboring binding spots by regular distances of $\sim 16 \pm 4$ Å. Table S1 shows the distance between adjacent binding spots on the Cse1p surface.

This regular and short spacing between binding spots is also observed in two other transport receptors. Both importin-β and NTF2 contain clusters of FG-repeat binding spots on their surfaces (Isgro and Schulten, 2005, 2007). Importin-β contains two clusters. One cluster is made up of four binding spots in the N-terminal half of the molecule between HEAT repeat 5 and 9. The other cluster is also

made up of four binding spots, but it is located in the C-terminal half of the molecule between HEAT repeat 14 and 17. Each of the four binding spots in the two clusters is separated by a distance of ~14 ± 3 Å (see Table S3), very similar to the distance between binding spots in the large Cse1p cluster. The surface of NTF2 also contains binding spots separated by similar short and regular distances to those of Cse1p and importin-β. The NTF2 binding spots, particularly #1 and #3–#6 (Isgro and Schulten, 2007), broadly form a stripe across the surface akin to the hydrophobic stripe identified by Morrison et al. (2003) due to the short and regular separation of binding spots. The distances between binding spots forming this broad stripe are ~11 ± 3 Å (see Table S4), and the distances between binding spots #2 and #5 and #2 and #6 are 16 Å each.

The multitude of binding spots separated by regular and short distances on the surfaces of Cse1p, importin-β, and NTF2 compared to that of Kap60p suggests that the NPC uses both binding spot number and proximity to determine whether a macromolecule (complex) is fit for transport. In distinguishing between legitimate transport receptors and inert molecules not destined to traverse the nuclear envelope alone, the NPC must utilize a mechanism that is capable of protecting against the random occurrence of a binding spot on the surface of an inert molecule that is capable of binding FG-nups. Indeed, any inert macromolecule may possess one or several hydrophobic depressions on its surface that are not explicitly used for nuclear transport, but are capable of FG-nup binding nonetheless. The binding of a single FG-repeat, or even a few, to the surface of a molecule is unlikely to render successful nuclear transport.

The NPC may protect against these "random" binding spots by requiring a transport receptor to have several binding spots in close proximity on its surface. With numerous and close binding spots on a transport receptor's surface, the NPC may be able to bind multiple FG-repeats to the transport receptor simultaneously, ensuring a strong enough composite binding energy to enable nuclear transport. Furthermore, the regular spacing between binding spots may be coordinated with the regular spacing between FG-repeats within individual FG-nups. Both spacings may be tuned to allow for the binding of FG-repeats to binding spots while also allowing the energetically favorable adherence of FG-nup linker regions to the transport receptor surface. Such a "tight fit" has already been observed experimentally in the binding of two FG-repeats from the same Nup1p peptide to the surface of yeast importin-β (Liu and Stewart, 2005). Liu and Stewart (2005) observe binding by two Nup1p Phe residues between HEAT repeats 6/7 and 7/8. The Phe residues are linked by 9 Nup1p residues that make intimate contact with the yeast importin-β surface. The binding of several FG-repeats from the same FG-nup may take place in vivo in an analogous way, exploiting the regularity in spacing of both binding spots on the transport receptor surface and that between FG-repeats. The regular spacing of binding spots into stripes, bands, or belts may effectively serve as a robust means for the NPC to identify transport complexes among a host of inert molecules that may possess hydrophobic patches on their surfaces. Future computational studies will further inspect the interactions between the NPC and transport complexes and will focus on the specificity and promiscuity of the binding spot:FG motif relationship and on the role of nonbinding segments of FG-nups.

EXPERIMENTAL PROCEDURES

The current work utilized molecular dynamics to study the association of FG-repeat peptides of varying length to the surface of the export complex Cse1p:Kap60p:RanGTP. Four separate binding simulations were performed in addition to equilibration of the export complex for a total simulation time of 165 ns. Each binding simulation contained over 250,000 atoms (see Table S5).

The 2.0 Å resolution X-ray crystallographic structure of the export complex (Matsuura and Stewart, 2004) (PDB code 1WA5) was used. The structure contains Cse1p and Kap60p from *Saccharomyces cerevisiae* and Ran from *Canis familiaris*. All missing residues from Cse1p, along with missing Kap60p residues 20–30, were added. Equilibration ensured the adoption of random coil configurations for these residues, and no large changes in overall secondary or tertiary structures were observed. Missing N- and C-terminal residues for Kap60p and missing N-terminal residues for Ran were not added. Missing Kap60p residues 59–86, which presumably adopt a random coil configuration away from the bulk of the export complex, were also not added.

The resulting structure was solvated in a water box measuring 132 × 129 × 153 $Å^3$ to ensure that the protein was 15 Å from the box edge and hence 30 Å from its periodic image. Na^+ and Cl^- ions were added to an ionic strength of 0.1 M. The entire structure contained 248,429 atoms (15,571 Cse1p atoms, 7,539 Kap60p atoms, 2,797 Ran atoms, 44 GTP atoms, 1 Mg^+ ion, 74,113 water molecules, 82 Na^+ ions, 56 Cl^- ions). The system was equilibrated according to the following protocol. All protein atoms were kept fixed, and the system was energy minimized for 5,000 steps, after which 200 ps of dynamics were run in an NVT ensemble (temperature = 298 K). The protein was then freed, the entire system was minimized for another 5,000 steps, and dynamics were run in the NPT ensemble (pressure = 1 atm) for 6.0 ns. After this time, the root-mean-square deviation (rmsd) of backbone Cα atoms settled around 2.1 Å for the complex as a whole compared to the crystal structure (Matsuura and Stewart, 2004) (see Figure S1) and 1.9 Å for Cse1p, 2.1 Å for Kap60, and 1.1 Å for Ran. The rmsd of the complex Cα atoms increased slightly over the course of binding simulations. These changes were due predominantly to regions at the ends of Kap60p and Cse1p that do not interact with the complex significantly. This high intrinsic flexibility of karyopherins has been documented (Conti et al., 2006) (see Figure S1).

The equilibrated export complex was used as a starting configuration for simulating the binding of FG-nups to its surface. Four separate binding simulations were continued from the equilibration simulation. In each simulation, short chains of FG-nups were added to the solution surrounding the equilibrated export complex. The added chains were either 4, 6, 8, or 10 amino acids in length, corresponding to simulations 1, 2, 3, and 4, respectively (see Table S5). In each simulation, 111 individual chains were added, yielding an FG-repeat concentration of ~60 mM. Simulation 1 exclusively used chains of sequence FSFG, while simulations 2, 3, and 4 used chain sequences taken from nups Nsp1 and Nup116 (see Table 1). The chains were added in a straight backbone configuration ($\phi = \psi = 180°$) at random positions and orientations in the surrounding solution. A new set of Na^+/Cl^- counterions was added to 0.1 M concentration. The new systems were each equilibrated as follows. All protein atoms were fixed, and the system was energy minimized for 3,000 steps, followed by 200 ps of dynamics in the NVT ensemble (T = 298 K). FG-nup peptides were then freed

from fixed constraints, while the export complex proteins were kept fixed. The system was minimized for 5,000 steps, followed by 500 ps of NVT ensemble dynamics. All atoms were then freed from constraints, the system was minimized again for 3,000 steps, and dynamics were run in the NPT ensemble (p = 1 atm) for the amount of time listed in Table S5.

All molecular dynamics simulations were performed by using the program NAMD 2.6 (Phillips et al., 2005) with the CHARMM27 forcefield for proteins and nucleic acids (MacKerell et al., 1998; Foloppe and MacKerrell, 2000; MacKerell and Banavali, 2000) and the TIP3P water model (Jorgensen et al., 1983). The simulations utilized periodic boundary conditions and the Particle Mesh Ewald (PME) method (Darden et al., 1993) to calculate electrostatic forces without cutoff. van der Waals interactions were calculated with a cutoff of 12 Å and a switching distance of 10 Å. A multiple timestepping algorithm (Grubmüller et al., 1991; Schlick et al., 1999) was utilized with a 1 fs step for bonded force evaluation, 2 fs for short-range nonbonded forces (within the cutoff), and 4 fs for long-range electrostatics (outside the cutoff). Langevin dynamics were used to control temperature by using a damping coefficient of 5 ps^{-1}; hydrogen atoms were not coupled to the heat bath. Pressure was regulated via the hybrid Nosé-Hoover (Martyna et al., 1994) Langevin (Feller et al., 1995) piston method by using a piston oscillation period of 100 fs and a damping timescale of 50 fs.

During the course of each binding simulation, FG-nup peptides interact with the surface of the Cse1p:Kap60p:RanGTP export complex. In order to determine which interactions could be classified as relevant in vivo, on the order of microseconds or milliseconds, a sequence conservation criterion was applied. Ten Cse1p (CAS) sequences were aligned from species *Saccharomyces cerevisiae*, *Schizosaccharomyces pombe*, *Homo sapiens*, *Pongo pygmaeus*, *Mus musculus*, *Xenopus laevis*, *Drosophila melanogaster*, *Oreochromis niloticus*, *Pagrus major*, and *Brachydanio rerio*. Nine Kap60p (importin-α) sequences were aligned from *Saccharomyces cerevisiae*, *Schizosaccharomyces pombe*, *Homo sapiens*, *Mus musculus*, *Rattus norvegicus*, *Arabidopsis thaliana*, *Xenopus laevis*, *Caenorhabditis elegans*, and *Oryza sativa*.

The sequences were aligned by using a set of GONNET matrices (Gonnet et al., 1992) and the Clustal sequence alignment program (Thompson et al., 1997). Each residue position within the alignment was scored from 0 to 100 based on its degree of conservation and the percent accepted mutation distance of other aligned residues. Then, if a residue was completely conserved and also hydrophobic, its score was increased to 130. This was done to highlight residues on the protein surface that may have been conserved due to their role in FG-nup binding, which should occur in hydrophobic pockets on the surface. Completely conserved tyrosine residues were also given a score of 130, reflecting the observation that tyrosine and phenylalanine residues both contain large aromatic rings that are capable of binding FG-nups in a similar way.

Simulation 1 with four amino acid long chains resulted in ten binding spots occupied, while the other simulations with longer chains resulted in only six spots occupied. This difference is likely due to the higher mobility of the shorter chains (in this case, the binding indeed occurred faster on average) and is possibly also due to more optimal binding of the FSFG motif over the other motifs explored, i.e., due to higher binding affinities. Given the limited statistics of the simulations carried out because of relatively short simulation times, binding affinities could not be calculated, as this would require monitoring on-and off-events. Future investigations may reveal the binding affinities through suitable, but computationally expensive, simulation algorithms, though the actual binding affinities will certainly be affected by contributions of entire NPC proteins, not only by their binding motifs.

Supplemental Data

Supplemental Data include a figure showing the rmsd of the Cse1p:Kap60p:RanGTP complex, five tables (four showing the distance between adjacent FG-nup binding spots on Cse1p, Kap60p, importin-β, and NTF2, respectively, and one summarizing the molecular dynamics simulations performed in the current study), and four movies (one showing a typical binding simulation performed, and three showing the location of FG-repeat binding spots on the surfaces of Cse1p, importin-β, and NTF2, respectively) and are available at http://www.structure.org/cgi/content/full/15/8/977/DC1/.

ACKNOWLEDGMENTS

The authors acknowledge support from National Institutes of Health grant P41RR05969. K.S. was supported by the Humboldt Foundation. The authors also gladly acknowledge supercomputer time provided by the National Center for Supercomputing Applications and the Pittsburgh Supercomputer Center through the National Science Foundation and the Large Resources Allocation Committee grant MCA93S028. All molecular images in this paper were prepared by using the molecular visualization software VMD (Humphrey et al., 1996).

Received: May 2, 2007
Revised: June 26, 2007
Accepted: June 27, 2007
Published: August 14, 2007

REFERENCES

Aebi, U., Jarnik, M., Reichelt, R., and Engel, A. (1990). Structural analysis of the nuclear pore complex by conventional and scanning transmission electron microscopy (CTEM/STEM). EMSA Bull. *20*, 69–76.

Akey, C.W., and Radermacher, M. (1993). Architecture of the *Xenopus* nuclear pore complex revealed by three-dimensional cryo-electron microscopy. J. Cell Biol. *122*, 1–19.

Bayliss, R., Ribbeck, K., Akin, D., Kent, H.M., Feldherr, C.M., Görlich, D., and Stewart, M. (1999). Interaction between NTF2 and xFxFG-containing nucleoporins is required to mediate nuclear import of RanGDP. J. Mol. Biol. *293*, 579–593.

Bayliss, R., Littlewood, T., and Stewart, M. (2000). Structural basis for the interaction between FxFG nucleoporin repeats and importin-β in nuclear trafficking. Cell *102*, 99–108.

Bayliss, R., Leung, S.W., Baker, R.P., Quimby, B.B., Corbett, A.H., and Stewart, M. (2002a). Structural basis for the interaction between NTF2 and nucleoporin FxFG repeats. EMBO J. *21*, 2843–2853.

Bayliss, R., Littlewood, T., Strawn, L.A., Wente, S.R., and Stewart, M. (2002b). GLFG and FxFG nucleoporins bind to overlapping sites on importin-β. J. Biol. Chem. *277*, 50597–50606.

Beck, M., Förster, F., Ecke, M., Plitzko, J., Melchior, F., Gerisch, G., Baumeister, W., and Medalia, O. (2004). Nuclear pore complex structure and dynamics revealed by cryoelectron tomography. Science *306*, 1387–1390.

Bednenko, J., Cingolani, G., and Gerace, L. (2003). Importin-β contains a COOH-terminal nucleoporin binding region important for nuclear transport. J. Cell Biol. *162*, 391–401.

Ben-Efriam, I., and Gerace, L. (2001). Gradient of increasing affinity of importin-β for nucleoporins along the pathway of nuclear import. J. Cell Biol. *152*, 411–417.

Bischoff, F., Klebe, C., Kretschmer, J., Wittinghofer, A., and Ponstingl, H. (1994). RanGAP1 induces GTPase activity of nuclear Ras-related Ran. Proc. Natl. Acad. Sci. USA *91*, 2587–2591.

Bischoff, F., Krebber, H., Kempf, T., Hermes, I., and Ponstingl, H. (1995a). Human RanGTPase-activating protein RanGAP1 is a homologue of yeast Rna1p involved in mRNA processing and transport. Proc. Natl. Acad. Sci. USA *92*, 1749–1753.

Bischoff, F., Krebber, H., Smirnova, E., Dong, W., and Ponstingl, H. (1995b). Coactivation of RanGTPase and inhibition of GTP dissociation by Ran-GTP binding protein RanBP1. EMBO J. *14*, 705–715.

Braun, I., Herold, A., Rode, M., and Izaurralde, E. (2002). Nuclear export of mRNA by TAP/NXF1 requires two nucleoporin-binding sites but not p15. Mol. Cell. Biol. *22*, 5405–5418.

Chaillan-Huntington, C., Braslavsky, C.V., Kuhlmann, J., and Stewart, M. (2000). Dissecting the interactions between NTF2, RanGDP, and the nucleoporin XFXFG repeats. J. Biol. Chem. *275*, 5874–5879.

Chi, N.C., and Adam, S.A. (1997). Functional domains in nuclear import factor p97 for binding the nuclear localization sequence receptor and the nuclear pore. Mol. Biol. Cell *8*, 945–956.

Clarkson, W.D., Kent, H.M., and Stewart, M. (1996). Separate binding sites on nuclear transport factor 2 (NTF2) for GDP-Ran and the phenylalanine-rich repeat regions of nucleoporins p62 and nsp1p. J. Mol. Biol. *263*, 517–524.

Conti, E., Müller, C., and Stewart, M. (2006). Karyopherin flexibility in nucleocytoplasmic transport. Curr. Opin. Struct. Biol. *16*, 237–244.

Cook, A., Fernandez, E., Lindner, D., Ebert, J., Schlenstedt, G., and Conti, E. (2005). The structure of the nuclear export receptor Cse1 in its cytosolic state reveals a closed conformation incompatible with cargo binding. Mol. Cell *18*, 355–367.

Cronshaw, J., Krutchinsky, A., Zhang, W., Chait, B., and Matunis, M. (2002). Proteomic analysis of the mammalian nuclear pore complex. J. Cell Biol. *158*, 915–927.

Cushman, I., Bowman, B., Sowa, M., Lichtarge, O., Quiocho, F., and Moore, M. (2004). Computational and biochemical identification of a nuclear pore complex binding site on the nuclear transport carrier NTF2. J. Mol. Biol. *344*, 303–310.

Damelin, M., and Silver, P.A. (2000). Mapping interactions between nuclear transport factors in living cells reveals pathways through the nuclear pore complex. Mol. Cell *5*, 133–140.

Darden, T., York, D., and Pedersen, L. (1993). Particle mesh Ewald. An N•log(N) method for Ewald sums in large systems. J. Chem. Physiol. *98*, 10089–10092.

Denning, D., and Rexach, M. (2007). Rapid evolution exposes the boundaries of domain structure and function in natively unfolded FG nucleoporins. Mol. Cell. Proteomics *6*, 272–282.

Denning, D.P., Patel, S.S., Uversky, V., Fink, A.L., and Rexach, M. (2003). Disorder in the nuclear pore complex: the FG repeat regions of nucleoporins are natively unfolded. Proc. Natl. Acad. Sci. USA *100*, 2450–2455.

Devos, D., Dokudovskaya, S., Alber, F., Williams, R., Chait, B., Sali, A., and Rout, M. (2004). Components of coated vesicles and nuclear pore complexes share a common molecular architecture. PLoS Biol. *2*, e380.

Devos, D., Dokudovskaya, S., Williams, R., Alber, F., Eswar, N., Chait, B., Rout, M., and Sali, A. (2006). Simple fold composition and modular architecture of the nuclear pore complex. Proc. Natl. Acad. Sci. USA *103*, 2172–2177.

Feller, S.E., Zhang, Y.H., Pastor, R.W., and Brooks, B.R. (1995). Constant pressure molecular dynamics simulation - the Langevin piston method. J. Chem. Physiol. *103*, 4613–4621.

Foloppe, N., and MacKerrell, A.D., Jr. (2000). All-atom empirical force field for nucleic acids: I. Parameter optimization based on small molecule and condensed phase macromolecular target data. J. Comp. Chem. *21*, 86–104.

Fornerod, M., van Deursen, J., van Baal, S., Reynolds, A., Davis, D., Murti, K., Fransen, J., and Grosveld, G. (1997). The human homologue of yeast CRM1 is in a dynamic subcomplex with CAN/Nup214 and a novel nuclear pore component Nup88. EMBO J. *16*, 807–816.

Fried, H., and Kutay, U. (2003). Nucleocytoplasmic transport: taking an inventory. Cell. Mol. Life Sci. *60*, 1659–1688.

Gilchrist, D., and Rexach, M. (2003). Molecular basis for the rapid dissociation of nuclear localization signals from karyopherin α in the nucleoplasm. J. Biol. Chem. *278*, 51937–51949.

Gilchrist, D., Mykytka, B., and Rexach, M. (2002). Accelerating the rate of disassembly of karyopherin•cargo complexes. J. Biol. Chem. *277*, 18161–18172.

Goldberg, M., Wiese, C., Allen, T., and Wilson, K. (1997). Dimples, pores, star-rings, and thin rings on growing nuclear envelopes: evidence for structural intermediates in nuclear pore complex assembly. J. Cell Sci. *110*, 409–420.

Gonnet, G.H., Cohen, M.A., and Benner, S.A. (1992). Exhaustive matching of the entire protein sequence database. Science *256*, 1443–1445.

Görlich, D., and Kutay, U. (1999). Transport between the cell nucleus and the cytoplasm. Annu. Rev. Cell Dev. Biol. *15*, 607–660.

Grote, M., Kubitscheck, U., Reichelt, R., and Peters, R. (1995). Mapping of nucleoporins to the center of the nuclear pore complex by post-embedding immunogold electron microscopy. J. Cell Sci. *108*, 2963–2972.

Grubmüller, H., Heller, H., Windemuth, A., and Schulten, K. (1991). Generalized Verlet algorithm for efficient molecular dynamics simulations with long-range interactions. Mol. Sim. *6*, 121–142.

Hood, J., and Silver, P. (1998). Cse1p is required for export of Srp1p/importin-α from the nucleus in *Saccharomyces cerevisiae*. J. Biol. Chem. *273*, 35142–35146.

Hopper, A., Traglia, H., and Dunst, R. (1990). The yeast RNA1 gene product necessary for RNA processing is located in the cytosol and apparently excluded from the nucleus. J. Cell Biol. *111*, 309–321.

Hu, T., Guan, T., and Gerace, L. (1997). Molecular and functional characterization of the p62 complex, an assembly of nuclear pore complex glycoproteins. J. Cell Biol. *134*, 589–601.

Humphrey, W., Dalke, A., and Schulten, K. (1996). VMD: visual molecular dynamics. J. Mol. Graph. *14*, 33–38.

Iovine, M.K., Watkins, J.L., and Wente, S.R. (1995). The GLFG repetitive region of the nucleoporin Nup116p interacts with Kap95p, an essential yeast nuclear import factor. J. Cell Biol. *131*, 1699–1713.

Isgro, T.A., and Schulten, K. (2005). Binding dynamics of isolated nucleoporin repeat regions to importin-β. Structure *13*, 1869–1879.

Isgro, T.A., and Schulten, K. (2007). Association of nuclear pore FG-repeat domains to NTF2 import and export complexes. J. Mol. Biol. *366*, 330–345.

Izaurralde, E., Kutay, U., von Kobbe, C., Mattaj, I.W., and Görlich, D. (1997). The asymmetric distribution of the constituents of the Ran system is essential for transport into and out of the nucleus. EMBO J. *16*, 6535–6547.

Jarnik, M., and Aebi, U. (1991). Toward a more complete 3-D structure of the nuclear pore complex. J. Struct. Biol. *107*, 291–308.

Jorgensen, W.L., Chandrasekhar, J., Madura, J.D., Impey, R.W., and Klein, M.L. (1983). Comparison of simple potential functions for simulating liquid water. J. Chem. Physiol. *79*, 926–935.

Kehlenbach, R.H., Dickmanns, A., Kehlenbach, A., Guan, T., and Gerace, L. (1999). A role for RanBP1 in the release of CRM1 from the nuclear pore complex in a terminal step of nuclear export. J. Cell Biol. *145*, 645–657.

Kiseleva, E., Goldberg, M., Allen, T., and Akey, C. (1998). Active nuclear pore complexes in *Chironomus*: visualization of transporter configurations related to mRNP export. J. Cell Sci. *111*, 223–236.

Kose, S., Imamoto, N., Tachibana, T., Yoshida, M., and Yoneda, Y. (1999). β-subunit of nuclear pore-targeting complex (importin-β) can be exported from the nucleus in a Ran-independent manner. J. Biol. Chem. *274*, 3946–3952.

Künzler, M., and Hurt, E. (1998). Cse1p functions as the nuclear export receptor for importin α in yeast. FEBS Lett. *433*, 185–190.

Kutay, U., Bischoff, F., Kostka, S., Kraft, R., and Görlich, D. (1997). Export of importin α from the nucleus is mediated by a specific nuclear transport factor. Cell *90*, 1061–1071.

Lane, C., Cushman, I., and Moore, M. (2000). Selective disruption of nuclear import by a functional mutant nuclear transport carrier. J. Cell Biol. *151*, 321–332.

Lee, S.J., Sekimoto, T., Yamashita, E., Nagoshi, E., Nakagawa, A., Imamoto, N., Yoshimura, M., Sakai, H., Chong, K.T., Tsukihara, T., et al. (2003). The structure of importin bound to SREBP-2: nuclear import of a transcription factor. Science *302*, 1571–1575.

Lim, R., Aebi, U., and Stoffler, D. (2006a). From the trap to the basket: getting to the bottom of the nuclear pore complex. Chromosoma *115*, 15–26.

Lim, R., Huang, N., Köser, J., Deng, J., Lau, K., Schwarz-Herion, K., Fahrenkrog, B., and Aebi, U. (2006b). Flexible phenylalanine-glycine nucleoporins as entropic barriers to nucleocytoplasmic transport. Proc. Natl. Acad. Sci. USA *103*, 9512–9517.

Lim, R.Y., Köser, J., Huang, N.P., Schwarz-Herion, K., and Aebi, U. (2007). Nanomechanical interactions of phenylalanine-glycine nucleoporins studied by single molecule force-volume spectroscopy. J. Struct. Biol., in press.

Liu, S.M., and Stewart, M. (2005). Structural basis for the high-affinity binding of nucleoporin Nup1p to the *Saccharomyces cerevisiae* importin-β homologue, Kap95p. J. Mol. Biol. *349*, 515–525.

Macara, I.G. (2001). Transport into and out of the nucleus. Microbiol. Mol. Biol. Rev. *65*, 570–594.

MacKerell, A.D., Jr., and Banavali, N.K. (2000). All-atom empirical force field for nucleic acids: II. Application to molecular dynamics simulations of DNA and RNA in solution. J. Comp. Chem. *21*, 105–120.

MacKerell, A., Jr., Bashford, D., Bellott, M., Dunbrack, R.L., Jr., Evanseck, J., Field, M.J., Fischer, S., Gao, J., Guo, H., Ha, S., et al. (1998). All-atom empirical potential for molecular modeling and dynamics studies of proteins. J. Phys. Chem. B *102*, 3586–3616.

Mahajan, R., Delphin, C., Guan, T., Gerace, L., and Melchior, F. (1997). A small ubiquitin-related polypeptide involved in targeting RanGAP1 to nuclear pore complex protein RanBP2. Cell *88*, 97–107.

Mansfeld, J., Güttinger, S., Hawryluk-Gara, L., Panté, N., Mall, M., Galy, V., Haselmann, U., Mühlhäusser, P., Wozniak, R., Mattaj, I., et al. (2006). The conserved transmembrane nucleoporin NDC1 is required for nuclear pore complex assembly in vertebrate cells. Mol. Cell *22*, 93–103.

Martyna, G., Tobias, D.J., and Klein, M.L. (1994). Constant pressure molecular dynamics algorithms. J. Chem. Physiol. *101*, 4177–4189.

Matsuura, Y., and Stewart, M. (2004). Structural basis for the assembly of a nuclear export complex. Nature *432*, 872–877.

Matsuura, Y., and Stewart, M. (2005). Nup50/Npap60 function in nuclear protein import complex disassembly and importin recycling. EMBO J. *24*, 3681–3689.

Matsuura, Y., Lange, A., Harreman, M., Corbett, A., and Stewart, M. (2003). Structural basis for Nup2p function in cargo release and karyopherin recycling in nuclear import. EMBO J. *22*, 5358–5369.

Matunis, M., Coutavas, E., and Blobel, G. (1996). A novel ubiquitin-like modification modulates the partitioning of the Ran-GTPase-activating protein RanGAP1 between the cytosol and the nuclear pore complex. J. Cell Biol. *135*, 1457–1470.

Moore, M.S. (1998). Ran and nuclear transport. J. Biol. Chem. *273*, 22857–22860.

Morrison, J., Yang, J., Stewart, M., and Neuhaus, D. (2003). Solution NMR study of the interaction between NTF2 and nucleoporin FxFG repeats. J. Mol. Biol. *333*, 587–603.

Mosammaparast, N., and Pemberton, L. (2004). Karyopherins: from nuclear-transport mediators to nuclear-function regulators. Trends Cell Biol. *14*, 547–556.

Nachury, M., and Weis, K. (1999). The direction of transport through the nuclear pore can be inverted. Proc. Natl. Acad. Sci. USA *96*, 9622–9627.

Nemergut, M., Mizzen, C., Stukenberg, T., Allis, C., and Macara, I. (2001). Chromatin docking and exchange activity enhancement of RCC1 by histones H2A and H2B. Science *292*, 1540–1543.

Ohtsubo, M., Kai, R., Furuno, N., Sekiguchi, T., Sekiguchi, M., Hayashida, H., Kuma, K., Miyata, T., Fukushige, S., and Murotsu, T. (1987). Isolation and characterization of the active cDNA of the human cell cycle gene (RCC1) involved in the regulation of onset of chromosome condensation. Genes Dev. *1*, 585–593.

Ohtsubo, M., Okazaki, H., and Nishimoto, T. (1989). The RCC1 protein, a regulator for the onset of chromosome condensation locates in the nucleus and binds to DNA. J. Cell Biol. *109*, 1389–1397.

Pante, N., and Kann, M. (2002). Nuclear pore complex is able to transport macromolecules with diameters of about 39 nm. Mol. Biol. Cell *13*, 425–434.

Paschal, B., and Gerace, L. (1995). Identification of NTF2, a cytosolic factor for nuclear import that interacts with nuclear pore complex protein p62. J. Cell Biol. *129*, 925–937.

Pemberton, L., and Paschal, B. (2005). Mechanisms of receptor-mediated nuclear import and nuclear export. Traffic *6*, 187–198.

Peters, R. (2005). Translocation through the nuclear pore complex: selectivity and speed by reduction-of-dimensionality. Traffic *6*, 421–427.

Phillips, J.C., Braun, R., Wang, W., Gumbart, J., Tajkhorshid, E., Villa, E., Chipot, C., Skeel, R.D., Kale, L., and Schulten, K. (2005). Scalable molecular dynamics with NAMD. J. Comp. Chem. *26*, 1781–1802.

Quimby, B., Leung, S., Bayliss, R., Harreman, M., Thirumala, G., Stewart, M., and Corbett, A. (2001). Functional analysis of the hydrophobic patch on nuclear transport factor 2 involved in interactions with the nuclear pore in vivo. J. Biol. Chem. *276*, 38820–38829.

Radu, A., Blobel, G., and Moore, M.S. (1995a). Identification of a protein complex that is required for nuclear protein import and mediates docking of import substrate to distinct nucleoporins. Proc. Natl. Acad. Sci. USA *92*, 1769–1773.

Radu, A., Moore, M.S., and Blobel, G. (1995b). The peptide repeat domain of nucleoporin Nup98 functions as a docking site in transport across the nuclear pore complex. Cell *81*, 215–222.

Rexach, M., and Blobel, G. (1995). Protein import into nuclei: association and dissociation reactions involving transport substrate, transport factors, and nucleoporins. Cell *83*, 683–692.

Ribbeck, K., and Görlich, D. (2001). Kinetic analysis of translocation through nuclear pore complexes. EMBO J. *20*, 1320–1330.

Richards, S.A., Carey, K.L., and Macara, I.G. (1997). Requirement of guanosine triphosphate-bound Ran for signal-mediated nuclear protein export. Science *276*, 1842–1844.

Rodriguez, M., Dargemont, C., and Stutz, F. (2004). Nuclear export of RNA. Biol. Cell *96*, 639–655.

Rout, M.P., and Blobel, G. (1993). Isolation of the yeast nuclear pore complex. J. Cell Biol. *123*, 771–783.

Rout, M.P., Aitchison, J.D., Suprapto, A., Hjertaas, K., Zhao, Y., and Chait, B.T. (2000). The yeast nuclear pore complex: composition, architecture, and transport mechanism. J. Cell Biol. *148*, 635–651.

Rout, M.P., Aitchison, J.D., Magnasco, M.O., and Chait, B.T. (2003). Virtual gating and nuclear transport: the hole picture. Trends Cell Biol. *13*, 622–628.

Saitoh, H., Sparrow, D., Shiomi, T., Pu, R., Nishimoto, T., Mohun, T., and Dasso, M. (1998). Ubc9p and the conjugation of SUMO-1 to RanGAP1 and RanBP2. Curr. Biol. *8*, 121–124.

Schlick, T., Skeel, R., Brünger, A., Kalé, L., Board, J.A., Jr., Hermans, J., and Schulten, K. (1999). Algorithmic challenges in computational molecular biophysics. J. Comp. Physiol. *151*, 9–48.

Schwartz, T. (2005). Modularity within the architecture of the nuclear pore complex. Curr. Opin. Struct. Biol. *15*, 221–226.

Seedorf, M., Damelin, M., Kahana, J., Taura, T., and Silver, P.A. (1999). Interactions between a nuclear transporter and a subset of nuclear pore complex proteins depend on Ran GTPase. Mol. Cell. Biol. *19*, 1547–1557.

Shah, S., Tugendreich, S., and Forbes, D. (1998). Major binding sites for the nuclear import receptor are the internal nucleoporin Nup153 and the adjacent nuclear filament protein Tpr. J. Cell Biol. *141*, 31–40.

Shulga, N., and Goldfarb, D.S. (2003). Binding dynamics of structural nucleoporins govern nuclear pore complex permeability and may mediate channel gating. Mol. Cell. Biol. *23*, 534–542.

Solsbacher, J., Maurer, P., Bischoff, F., and Schlenstedt, G. (1998). Cse1p is involved in export of yeast importin α from the nucleus. Mol. Cell. Biol. *18*, 6805–6815.

Stewart, M. (2007). Molecular mechanism of the nuclear protein import cycle. Nat. Rev. Mol. Cell Biol. *8*, 195–208.

Stoffler, D., Feja, B., Fahrenkrog, B., Walz, J., Typke, D., and Aebi, U. (2003). Cryo-electron tomography provides novel insights into nuclear pore architecture: implications for nucleocytoplasmic transport. J. Mol. Biol. *328*, 119–130.

Strawn, L.A., Shen, T., and Wente, S.R. (2001). The GLFG regions of Nup116p and Nup100p serve as binding sites for both Kap95p and Mex67p at the nuclear pore complex. J. Biol. Chem. *276*, 6445–6452.

Strawn, L.A., Shen, T., Shulga, N., Goldfarb, D.S., and Wente, S.R. (2004). Minimal nuclear pore complexes define FG repeat domains essential for transport. Nat. Cell Biol. *6*, 197–206.

Thompson, J.D., Gibson, T.J., Plewniak, F., Jeanmougin, F., and Higgins, D.G. (1997). The clustalx windows interface: flexible strategies for multiple sequence alignment aided by quality analysis tools. Nucleic Acids Res. *25*, 4876–4882.

Tran, E., and Wente, S. (2006). Dynamic nuclear pore complexes: life on the edge. Cell *125*, 1041–1053.

Weis, K. (2003). Regulating access to the genome: nucleocytoplasmic transport throughout the cell cycle. Cell *112*, 441–451.

Yang, Q., Rout, M., and Akey, C. (1998). Three-dimensional architecture of the isolated yeast nuclear pore complex: functional and evolutionary implications. Mol. Cell *1*, 223–234.